SUSD2 suppresses lung adenocarcinoma tumorigenesis by inducing autophagy *via* inhibiting PI3K/AKT/mTOR signaling pathway

Shengwen Wang,[1,2] Gang Yang,[3] Qian Zhang,[2] Yanbei Zhang[1]

[1]Lung Cancer Diagnosis and Treatment, Department of Geriatric Respiratory and Critical Care Medicine, The First Affiliated Hospital of Anhui Medical University, Hefei

[2]Department of Geriatric Medicine, Wuhu Hospital Affiliated to East China Normal University (Second People's Hospital of Wuhu City), Wuhu

[3]Department of Respiratory Medicine, Wuhu Hospital Affiliated to East China Normal University (Second People's Hospital of Wuhu City), Wuhu, China

ABSTRACT

Lung adenocarcinoma (LUAD) is the most common and aggressive non-small cell lung cancer with limited therapeutic options. SUSD2 exhibits varying regulatory behaviors in different types of tumors, its role in LUAD remains unclear. This study aims to determine the role of SUSD2 in LUAD and explore the underlying mechanism. Through TCGA database analysis, we discovered that SUSD2 expression is significantly downregulated in LUAD tissues, and its low expression is closely associated with advanced disease stages and poor patient prognosis. Further immunohistochemical validation confirmed reduced SUSD2 expression in clinical samples. Functional assays demonstrated that SUSD2 overexpression markedly inhibits LUAD cell proliferation, migration, and invasion, and also suppresses tumor growth and metastasis in mouse models. Mechanistic studies revealed that SUSD2 overexpression promotes autophagic flux (indicated by increased LC3-II and decreased p62) and suppresses the PI3K/AKT/mTOR signaling pathway. The antitumor effects of SUSD2 were attenuated by the autophagy inhibitor 3-MA or ATG5 knockdown, while reactivation of mTOR reversed SUSD2-induced autophagy and tumor suppression. In summary, SUSD2 functions as a tumor suppressor in LUAD by inducing autophagy and inhibiting the PI3K/AKT/mTOR pathway, suggesting its potential as a therapeutic target and prognostic biomarker.

Key words: SUSD2; LUAD; autophagy; tumor suppressor; cell proliferation; apoptosis.

Correspondence: Yanbei Zhang, PhD, Lung Cancer Diagnosis and Treatment, Department of Geriatric Respiratory and Critical Care Medicine, The First Affiliated Hospital of Anhui Medical University, 218 Jixi Road, Shushan District, Hefei 230022, China. E-mail: zhangyanbei@ahmu.edu.cn

Contributions: Shengwen Wang, cell-based experiments, animal experiments, experimental datasets validation, writing – original drafting. Gang Yang, bioinformatic analysis. Qian Zhang, immunohistochemistry analysis of clinical lung adenocarcinoma specimens, downstream signaling pathway validation. Yanbei Zhang, experimental protocols design, quality assurance procedures standardization. All the authors read and approved the final version of the manuscript and agreed to be accountable for all aspects of the work.

Conflict of interest: the authors declare no competing interests, and all authors confirm accuracy

Ethics approval: this study was approved by the Ethics Committee of Wuhu Second People's Hospital (Approval no.: 2024-KY-225) and conducted in accordance with the Declaration of Helsinki. Informed consent forms for all pathological specimens were signed by the patients themselves. All animal experiments were performed in accordance with the Guide for the Care and Use of Laboratory Animals and approved by the IACUC of Wuhu Second People's Hospital.

Availability of data and materials: all data generated or analyzed during this study are included in this published article.

Funding: this study was supported by the 2021 Anhui Provincial Key Medical and Health Specialty Construction Project (Respiratory Medicine) and the 2021 Wuhu Huatuo Plan Project.

Introduction

Lung adenocarcinoma (LUAD) represents the most prevalent histological subtype of non-small cell lung cancer (NSCLC) and is the leading cause of lung cancer-related mortality worldwide.[1] Due to its often asymptomatic early stages, LUAD is frequently diagnosed at an advanced stage, resulting in limited treatment efficacy and poor clinical prognosis.[2] However, while targeted therapies and immune checkpoint blockade have achieved monumental successes, the 5-year survival rate for advanced LUAD remains below 20%, which underscores the urgent need for novel therapeutic strategies and deeper mechanistic insights.[3] Therefore, elucidating the molecular mechanisms underlying LUAD initiation and progression, as well as identifying new prognostic markers and therapeutic targets, holds considerable clinical significance.

Autophagy is a highly conserved lysosomal degradation pathway that maintains cellular homeostasis by clearing dysfunctional or redundant cellular components through lysosomal activity, and is critical for cancer pathogenesis. And it restrains tumor initiation by maintaining genomic stability and cellular homeostasis. Conversely, autophagy can also promote tumor progression by facilitating cancer cells' survival under metabolic, oxidative, or therapeutic stress.[4,5] Mitophagy, a selective form of autophagy responsible for removing damaged mitochondria, helps prevent mitochondrial dysfunction and accumulation of reactive oxygen species. Therefore, impaired mitophagy has been increasingly linked to malignant transformation and metastasis.[6,7]

SUSD2 is an integral membrane protein associated with cell adhesion and signaling, which is involved in multiple oncogenic processes, such as cell proliferation, migration, immune evasion, and epithelial-mesenchymal transition (EMT).[8,9] Although SUSD2 overexpression is strongly associated with metastasis and unfavorable prognosis of NSCLC, its function of autophagy, especially mitophagy, remains largely unexplored.[10]

With diverse analytical methods, SUSD2 has been proven as a novel regulator of autophagy and facilitates autophagic activity in LUAD tumors, thereby it could suppress tumor cell survival and metastatic potential.[11] Not only do these findings reveal the new function of SUSD2 during the regulation of autophagy, but they also suggest the possibility as a therapeutic target for LUAD.[12]

Materials and Methods

Bioinformatics analysis

In the study, we utilized a series of bioinformatics analyses and websites to comprehensively evaluate SUSD2 expression and clinical relevance. RNA sequencing (RNA-seq) data and clinical information from 483 LUAD samples and 59 adjacent non-tumor tissues were obtained from The Cancer Genome Atlas (TCGA) database (http://portal.gdc.cancer.gov/; accessed on January 1, 2024). Batch effects were assessed and corrected using the ComBat method implemented in the SVA R package to account for systematic variations introduced by different sequencing platforms and sample processing batches. Raw count data were normalized using upper quartile normalization followed by log2 transformation to reduce technical variability. Differential expression of SUSD2 was visualized using box plots. Kaplan-Meier survival analysis and log-rank tests were performed based on TCGA-LUAD clinical data, with patients stratified into two categories according to the median SUSD2 expression level: a high expression group and a low expression group. The correlation between SUSD2 expression and clinical outcomes was evaluated, and receiver operating characteristic (ROC) curve analysis was applied to compare SUSD2 expression between LUAD and matched normal lung tissues. The area under the curve (AUC) was calculated to quantify the discriminatory capacity of SUSD2. To further investigate the molecular mechanisms involving SUSD2 in LUAD, Gene Set Enrichment Analysis (GSEA) was performed using GSEA software (v4.3.0; https://www.gsea-msigdb.org/gsea/index.jsp). Besides, a protein-protein interaction (PPI) network was constructed in the STRING database (https://string-db.org/; accessed on January 1, 2024) and visualized in Cytoscape (v3.9.1) to elucidate functions and molecular mechanisms of SUSD2 in LUAD. To systematically investigate the potential biological roles of SUSD2-associated genes, Gene Ontology (GO) and Kyoto Encyclopedia of Genes and Genomes (KEGG) enrichment analyses were performed on both up-regulated and down-regulated genes.

Clinical sample collection

This study included 40 pairs of tumor tissues and adjacent normal lung tissues from LUAD patients, collected in 2024 at Wuhu Second People's Hospital. *Supplementary Table 1* provides detailed clinical information for each patient, including pathological number, gender, age, hospitalization number, admission and discharge time, and tumor stage. This study was approved by the Ethics Committee of Wuhu Second People's Hospital (Approval No. 2024-KY-225) and conducted in accordance with the ethical guidelines of the Declaration of Helsinki. Prior to sample collection, written informed consent was obtained from all participants. Each tissue specimen was divided into two portions: one was fixed and embedded for histopathological examination, and the other was snap-frozen and stored in liquid nitrogen for subsequent molecular analysis.

Immunohistochemistry

Tissue samples were paraffin-embedded and sectioned at 4 μm thickness using a microtome. Sections were deparaffinized in xylene, rehydrated through a graded ethanol series, and rinsed with phosphate-buffered saline (PBS). Antigen retrieval was performed by microwave heating in citrate buffer (pH 6.0) at 95°C for 15 min, then cooled to room temperature. To block nonspecific binding, sections were incubated with 5% bovine serum albumin (BSA) for 30 min. Subsequently, slides were incubated overnight at 4°C in a humidified chamber with a rabbit anti-human SUSD2 primary antibody (Cat# bs-2850R; Bioss Inc., Woburn, MA, USA), diluted 1:200. After three washes with PBS (5 min each), sections were incubated at room temperature for 1 h at room temperature with a horseradish peroxidase (HRP)-conjugated secondary antibody (Cat# B001; Ebiogo, Hefei, China). Color development was performed using a 3,3'-Diaminobenzidine (DAB) substrate (Cat# B011; Ebiogo), with the reaction monitored under a microscope and terminated by rinsing with PBS. Finally, nuclei were counterstained with hematoxylin. Staining results were evaluated independently by two pathologists blinded to the clinicopathological data. A dual semi-quantitative scoring system was employed:[13] staining intensity was scored as 0 (negative), 1 (weak), 2 (moderate), or 3 (strong); the proportion of positive cells was scored as 0 (0%), 1 (1-10%), 2 (11-50%), 3 (51-80%), or 4 (81-100%). The composite score was calculated as the product of the intensity score and the proportion score, resulting in a final score ranging from 0 to 12. This composite score was used for statistical comparisons between LUAD tissues and adjacent normal tissues. Images were acquired and quantified using ImageJ software (v1.53) to assist in the analysis.

Cell culture and transfection

This study utilized the human normal bronchial epithelial cell lines BEAS-2B, along with human lung adenocarcinoma cell lines A549, H1299, H2228 and PC9. All cell lines were obtained from the American Type Culture Collection (ATCC, Manassas, VA, USA). Cells were maintained in RPMI-1640 medium (C11875500BT; Gibco, Waltham, MA, USA), supplemented with 10% fetal bovine serum (FBS; C10010500BT; Gibco) and 1% penicillin-streptomycin (15140122; Gibco), and incubated at 37°C in a humidified atmosphere. To establish stable SUSD2-overexpressing cell models, H1299 and H2228 cells were infected with lentiviral particles carrying the SUSD2 overexpression (SUSD2-OE) and an empty vector, both purchased from HeYuan Biotechnology (Shanghai, China). Each lentiviral construct co-expressed green fluorescent protein (GFP) and the puromycin resistance gene. Cells in the logarithmic growth phase were digested with trypsin and resuspended in complete culture medium to a density of 1×10^5 cells/mL. A total of 2×10^5 cells were seeded per well in 6-well plates (2 mL per well) and cultured overnight in a CO_2 incubator. Infection was performed when the cell fusion degree reached 60-70%. Polybrene (5 μg/mL, C0351; Beyotime Biotechnology, Shanghai, China) was added to the medium to enhance transduction efficiency of virus infection. Lentiviral particles were then introduced at a multiplicity of infection (MOI) of 10. Following 6-8 h of infection, the medium was replaced with fresh complete medium (2 mL/well). After 48 h of further culture, GFP expression was examined under a fluorescence microscope. Once the proportion of GFP-positive cells exceeded 70%, cells were harvested for subsequent experiments.

siRNA transfection

To knock down SUSD2 expression, small interfering RNA (siRNA) was used for transfection. The siRNAs were purchased from HeYuan Biotechnology. Thirty minutes prior to transfection, the culture medium in six-well plates was replaced with 1 mL of complete medium containing serum and antibiotics. A 100 pmol aliquot of siRNA was diluted in 250 μL of serum-free medium and gently mixed by pipetting or brief vortexing. Separately, 3 μL of NanoTrans transfection reagent (RK001002; Biomedical) was diluted in 250 μL of serum-free medium and gently mixed by pipetting three to four times. The diluted NanoTrans reagent was immediately added in its entirety to the diluted siRNA solution, mixed by three pipetting strokes or brief vortexing, and incubated at room temperature for 15 min to allow formation of NanoTrans-RNA complexes. The complexes were added dropwise to the medium in each well, and the plate was gently swirled to ensure uniform distribution. At 8 h post-transfection, the medium containing the complexes was removed and replaced with fresh complete medium containing serum and antibiotics. The cells were cultured for an additional 24 h before being collected for subsequent experiments.

Cell proliferation assay

In order to assess cell proliferation, we used the Cell Counting Kit-8 (CCK-8) assay. Cell in the logarithmic growth phase were trypsinized, resuspended, and seeded into 96-well plates at a density of 2,000 cells per well in 100 μL medium. Proliferation was measured daily for five consecutive days (days 1-5). Meanwhile, 10 μL of CCK-8 reagent (B1099; Biogenetech, Hefei, China) was added to each well, followed by incubation for 2 h at 37°C. A microplate reader was used at 450 nm to measure absorbance.

Wound healing assay

To evaluate migratory capacity, the wound healing assay was performed. Briefly, cells in the logarithmic growth phase were seeded into 6-well plates at an appropriate density. Upon reaching approximately 90% confluence, a uniform scratch was created across the monolayer using a sterile 10 μL pipette tip. After gently washing twice with PBS to remove detached cells, the medium was replaced with serum-free formulation. Images of the same field were captured at 0, 12, 24, and 48 h after scratching using an inverted microscope (Olympus IX73). Data analysis was carried out using ImageJ software (v1.53, National Institutes of Health, Bethesda, MD, USA), and the wound healing rate was calculated as follows: healing rate (%) = (initial scratch area – scratch area at each time point)/initial scratch area × 100%. Each experiment was performed in triplicate and repeated independently three times.

Colony formation assay

A colony formation assay was performed to evaluate the proliferative and colony-forming ability of cells *in vitro*. Cells in the logarithmic growth phase were trypsinized to generate a single-cell suspension, resuspended in complete culture medium to obtain single-cell suspensions, counted, and seeded into 6-well plates at a density of 600 cells per well. Each well was supplemented with 2 mL of complete medium, and the plate was gently shaken to ensure uniform cell distribution. Cells were cultured in a 37°C, 5% CO_2 incubator for 14 days, with medium replacement every three days. Colony growth was periodically monitored under a microscope. After the culture, the medium was discarded and the cells were gently washed twice with pre-cooled PBS. Subsequently, cells were fixed with 1 mL of 4% paraformaldehyde per well at room temperature for 15 min, followed by two PBS washes. Fixed colonies were stained with 1 mL of 0.1% crystal violet per well for 20 min at room temperature. The staining solution was then removed, and plates were rinsed multiple times with double-distilled water (ddH_2O) until the background was clear. Plates were air-dried at room temperature. Images of the stained colonies were captured using a digital camera, and colony numbers were quantified.

Transwell (non-ECM) invasion assay

Cell invasion ability was assessed *in vitro* using Transwell chambers (Cat# 3450; Corning Inc., Corning, NY, USA). Each chamber was placed into a 24-well plate, and 100 μL of serum-free medium was added to the upper chamber, followed by incubation at 37°C for 1 h to equilibrate the membrane. Cells in the logarithmic growth phase were digested, counted, and adjusted to a density of 6×10^4 cells per well. Then, 100 μL of the cell suspension was added to the upper chamber, while 600 μL of medium containing 20% FBS was added to the lower chamber. Cells were incubated at 37°C in a 5% CO_2 atmosphere for 48 h. After incubation, the chambers were carefully removed. Non-invasive cells remaining on the upper surface of the membrane were gently removed with a cotton swab. Chambers were fixed with 4% paraformaldehyde (Cat# E672002-0100; Sangon Biotech, Shanghai, China) at room temperature for 30 min, washed three times with PBS, and stained with 0.1% crystal violet staining solution (Cat# C0775; Sigma-Aldrich, St. Louis, MO, USA) for 30 min at room temperature. After staining, chambers were washed three times with PBS (C10010500BT; Gibco), after which chambers were air-dried. Three random fields per chamber were imaged under a microscope at 100 × magnification, and the number of invaded cells was counted.

Apoptosis assay

Apoptosis was analyzed by flow cytometry using the Annexin V-APC/7-AAD Apoptosis Detection Kit (KGA1106-100; KeyGEN BioTECH, Nanjing, China). As the cells in the 6-well plates had attained approximately 70%, we harvested the supernatant to retain suspended cells. Adherent cells were digested with trypsin, resuspended in complete medium, and combined with the corresponding supernatant in the same 15 mL centrifuge tube. Cells were centrifuged at 1300 rpm and 4°C for 5 min so as to discard the supernatant. We utilized pre-cooled PBS (4°C) to wash the cell pellet and resuspended the cells in 500 µL of Binding Buffer to obtain a single-cell suspension, and adjusted the concentration to 1×10^6 cells/mL. Then, 5 µL of Annexin V-APC and 5 µL of 7-AAD were added, followed by gentle mixing and incubation in the dark at room temperature for 10 min. Subsequently, 400 µL of pre-cooled 1x binding buffer was added, gently shaken, and detected by flow cytometry within 1 h. Every group performed three times.

qRT-PCR

Total RNA was extracted from cells using the AG RNAex Pro RNA Extraction Kit (Cat# AG21102; Accurate Biology, Changsha, China), with its concentration and purity determined by an Implen NanoPhotometer® Ultra-Micro UV-Vis Spectrophotometer (Implen GmbH, Munich, Germany). The cDNA was reversely transcribed using Evo M-MLV Reverse Transcriptase (Cat# AG11711; Accurate Biology) with random primers. qRT-PCR was performed on a StepOnePlus™ Real-Time PCR System (Applied Biosystems, Thermo Fisher Scientific, Waltham, MA, USA) using 2X SYBR Green Pro Taq HS Premix (Cat# AG11701; Accurate Biology). Each reaction was run in triplicate, along with a no-template negative control, every group performed three times. The relative gene expression levels were normalized to GAPDH as the internal reference and calculated using the $2^{(-\Delta\Delta Ct)}$ method. The following primers were used in the qRT-PCR experiments: GAPDH (GenBank Accession No. 2597) forward: GGAGCGAGATCCCTCCAAAAT, reverse: GGCTGTTGTCATACTTCTCATGG (product size: 197 bp, annealing temperature: 61.6°C); and SUSD2 (GenBank Accession No. 56241) forward: CACTGTGTCACTGGACAACG, reverse: GTGCCGTAGTATTGCCAACG (product size: 129 bp, annealing temperature: 61°C).

Western blot

Cells were washed with pre-cooled PBS and lysed on ice for 30 min using RIPA lysis buffer (R0010; Solarbio, Beijing, China) supplemented with protease and phosphatase inhibitors. Lysates were collected and centrifuged at 12,000 g for 15 min at 4°C to obtain the supernatant. Total protein concentration was quantified *via* a BCA kit (P0010; Beyotime Biotechnology). Equal amounts of protein (typically 20-40 µg) were mixed with loading buffer, denatured by boiling for 5 min, and separated by SDS-PAGE and transferred to PVDF membranes (IPVH00010; MilliporeSigma, Burlington, MA, USA) under constant current conditions. The membrane was blocked in TBST containing 5% BSA at room temperature for 2 h. Primary antibody incubation proceeded overnight at 4°C. Following three 10-min washes with TBST, the membranes were exposed to HRP-conjugated secondary antibodies for 1 h at room temperature, followed by another three TBST washes. Signal detection was carried out with an ECL system (Bio-Rad Laboratories, Hercules, CA, USA), and band intensity was quantified with ImageJ software (v1.53), and GAPDH was used as the loading control for normalizing target protein expression.

Transmission electron microscopy

To examine cellular ultrastructure, transmission electron microscopy (TEM) was performed. Cells were harvested and washed with pre-cooled 0.1 M PBS (pH 7.4), followed by fixation overnight at 4°C in 2.5% glutaraldehyde. After three 15-min PBS washes, and then made use of post-fixation samples were post-fixed in 1% osmium tetroxide for 4°C 2 h. Samples were then rinsed with PBS and dehydrated through a graded alcohols series (15 min per step). Following dehydration, the samples were treated with propylene oxide and gradually infiltrated with epoxy resin (Epon 812), then polymerized at 37°C, 45°C, and 60°C. Ultra-thin sections (70 nm) were cut employing an ultramicrotome and subjected to staining with uranyl acetate and lead citrate. And the images were recorded on the transmission electron microscope (JEM1400; JEOL Ltd., Tokyo, Japan).

Autophagy inhibitor

To investigate the role of SUSD2 in autophagy regulation, the classical autophagy 3-methyladenine (3-MA, Cat# HY-19312; MedChemExpress, Monmouth Junction, NJ, USA) was dissolved in sterile PBS to prepare a 100 mM stock solution and stored at -20°C. For experimental use, the stock solution was diluted to a final working concentration of 10 mM in complete culture medium. Cells were treated with 10 mM 3-MA for 24 h before subsequent assays.

Autophagic flux assay

H1299 and H2228 cells in logarithmic growth phase were digested with trypsin, resuspended in complete medium, and counted. A total of 4×10^5 cells were seeded per well into 6-well plates and incubated overnight at 37°C until cell confluence reached approximately 60-70%. Thirty minutes before transfection, the medium was replaced with 1 mL of complete medium containing serum and antibiotics. For each well, 10.4 µg of mCherry-GFP-LC3 plasmid (H35627; HeYuan Biotechnology) and 5.2 µg of SUSD2 plasmid (G0301245; General Biologicals, Chuzhou, China) were diluted in 132 µL of serum-free DMEM and mixed thoroughly. Separately, 6 µL of NanoTrans transfection reagent (RK001003; Biogenetech) was diluted in another 132 µL of serum-free DMEM. The two solutions were then combined and incubated at room temperature for 10 min to allow formation of NanoTrans-DNA complexes. The resulting transfection complex was gently added dropwise to each well, followed by gentle mixing. Cells were incubated for 16 h before replacing the medium with fresh RPMI-1640 complete medium. After 48 h of transfection, 10 mM 3-MA was added to both H1299 and H2228 cells for 24 h to inhibit autophagy. Cells were then observed and imaged using a Nikon Microscope Imaging System (Nikon DS-U3; Nikon, Tokyo, Japan) to evaluate autophagic flux via mCherry-GFP-LC3 fluorescence. Autophagic flux was evaluated based on the colocalization and signal patterns of mCherry (red) and GFP (green): yellow puncta ($mCherry^+/GFP^+$) represented autophagosomes, whereas red-only puncta ($mCherry^+/GFP^-$) indicated autolysosomes. The numbers of autophagosomes and autolysosomes per cell were quantified with ImageJ software (v1.53).

Animal experiments

All animal experiments were performed in accordance with institutional guidelines for animal welfare and ethics, and approved by the Medical Ethics Committee and the Institutional Animal Care and Use Committee (IACUC) of Wuhu Second People's Hospital (Approval No. 2024-KY-225). Male immunodeficient BALB/c-nu/nu nude mice (4-6 weeks old, n=10) were pur-

chased from Shanghai SLAC Laboratory Animal Co., Ltd. (Animal License No. SCXK (Hu) 2017-0005). Mice were housed under specific pathogen-free (SPF) conditions, with room temperature maintained at 22±2°C, relative humidity 50-60%, and a 12-h light/dark cycle. Food and water were provided ad libitum. Tumor modeling was performed by digesting H2228 NC and OE group cells in logarithmic growth phase with trypsin, resuspending in complete medium. The cell suspension was mixed 1:1 with pre-cooled Matrigel, and the final cell concentration was adjusted to 5×10^7 cells/mL. The mice were randomly divided into two groups, the vector control group and the SUSD2 overexpression group (n=5). 200 μL cell suspension was subcutaneously injected into the right flank area of each mouse in the corresponding group, followed by measurement of tumor size and body weight beginning from day 14 post-injection, and every 3 days thereafter. Tumor volume was calculated using the formula: volume = (length × width²)/2. Blind measurement was carried out by unknown group of experimental personnel. The general health and activity of the animals were monitored throughout the study. At the experimental endpoint (4 weeks post-injection), mice were anesthetized with isoflurane and euthanized by cervical dislocation. Subcutaneous tumors were completely excised, photographed, and weighed. Tumor tissues were snap-frozen in liquid nitrogen and stored at -80°C for subsequent molecular and histological analyses.

Hematoxylin and eosin staining

Paraffin-embedded tissue wax blocks were taken and serially sectioned (4 μm) using a microtome. After dewaxing and rehydration, the sections were immersed in hematoxylin staining solution for 3 min, then immersed in eosin staining solution for 1 min, followed by gradient dehydration and xylene transparent treatment. Neutral resin sealing agent was added dropwise, and histopathological evaluation was performed under an optical microscope and images were collected.

Statistical analysis

All statistical analyses were performed using SPSS software (version 15.0; SPSS Inc., USA) and R language (version 4.0.3; R Foundation, Austria). Quantitative data are expressed as mean ±SEM. Normality of data distribution was assessed using the Shapiro-Wilk test. For comparisons between two independent groups, the independent-samples *t*-test or Mann-Whitney *U* test was applied. For paired samples, the paired *t*-test or Wilcoxon signed-rank test was used. The Kaplan-Meier method and log-rank test were applied to assess the relationship between SUSD2 expression and patient prognosis in LUAD. This work applied ROC curve analysis to assess the diagnostic value of SUSD2 expression in differentiating LUAD tissues from adjacent normal lung tissues, AUC with its 95% confidence interval was calculated. All experiments were performed with three independent biological replicates. A p-value <0.05 was statistically significant.

Results

SUSD2 is down-regulated in LUAD and serves as a potential diagnostic and prognostic biomarker

Analysis of public datasets revealed that expression of SUSD2 was significantly down-regulated in LUAD tissues compared with adjacent normal tissues (p<0.001; Figure 1 A,B). To further evaluate the diagnostic value of SUSD2 in LUAD, ROC curve analysis was performed. The results demonstrated a strong diagnostic ability of SUSD2 to distinguish LUAD from normal tissues, with AUC of 0.940 (95% CI: 0.921-0.959; Figure 1C), indicating good discriminatory performance. Subgroup analyses proved that lower SUSD2 expression was closely correlated with higher pathological T stage (p<0.001; Figure 1D), whereas no marked differences were shown among different N or M stages (Figure 1 E,F). Kaplan-Meier survival analyses indicated that low SUSD2 expression was significantly correlated with poorer prognosis in LUAD patients, including reduced overall survival (OS; p=0.012; Figure 1G), disease-specific survival (DSS; p=0.019 Figure 1H), and progression-free interval (PFI; p=0.012; Figure 1I). Additionally, to validate SUSD2 expression in clinical specimens, we performed immunohistochemical staining on 40 paired LUAD and adjacent normal tissues. Consistent with the bioinformatics findings, SUSD2 protein levels were significantly lower in LUAD tissues than normal lung tissues (p<0.001; Figure 1J). Collectively, these results indicate that SUSD2 is downregulated in LUAD and is closely associated with tumor progression and unfavorable prognosis, suggesting its potential as a diagnostic and prognostic biomarker for LUAD.

Increased SUSD2 expression promotes autophagy in LUAD

The results of GSEA revealed that SUSD2 is significantly enriched in autophagy-related pathways in LUAD (Figure 2A), suggesting that SUSD2 may play an important role in the regulation of autophagy. To further validate this finding, we first assessed the baseline expression of SUSD2 in a normal bronchial epithelial cell line (BEAS-2B) and four lung adenocarcinoma cell lines (A549, PC9, H1299, and H2228) using qRT-PCR and Western blot. The results showed that SUSD2 mRNA and protein levels were significantly up-regulated in A549 and PC9 cells but down-regulated in H1299 and H2228 cells compared with BEAS-2B (Figure 2 B,C). Given that both bioinformatics analyses and clinical lung adenocarcinoma tissue samples indicated low SUSD2 expression, we selected the H1299 and H2228 cell lines for subsequent functional experiments. We first performed SUSD2 overexpression transfection in H1299 and H2228 cells and confirmed the transfection efficiency by qPCR (Figure 2D) and WB (Figure 2E). Meanwhile, we performed SUSD2 knockdown in A549 and PC9 cells, which endogenously express high levels of SUSD2, and confirmed the knockdown efficiency by qPCR and western blotting (*Supplementary Figure 1 A-D*). To investigate whether SUSD2 overexpression induces autophagy, TEM, WB, and immunofluorescence (IF) staining were performed. IF staining demonstrated that autophagic flux was significantly enhanced in the SUSD2 overexpression group compared to the Vector group, while it was markedly suppressed in the 3-MA-treated group. Notably, in both H1299 and H2228 cell lines, the 3-MA + SUSD2-OE group exhibited partial suppression of autophagic flux compared to the SUSD2-OE group (Figure 2F). TEM further confirmed these findings at the ultrastructural level, showing an increased number of autophagosomes in the SUSD2-OE group compared to the Vector group, a decreased number in the 3-MA group, and a notable decrease in autophagosome formation in the 3-MA + SUSD2-OE group relative to SUSD2-OE treatment alone (Figure 2G). WB analysis showed that the SUSD2-OE group significantly decreased the level of the autophagy substrate P62 while up-regulating Beclin-1 expression and increasing the LC3B-II/I ratio, indicative of enhanced autophagic flux. These changes were reversed by 3-MA treatment, which promoted P62 accumulation, down-regulated Beclin-1, and reduced the LC3B-II/I ratio. The autophagy-promoting effect of SUSD2 overexpression was attenu-

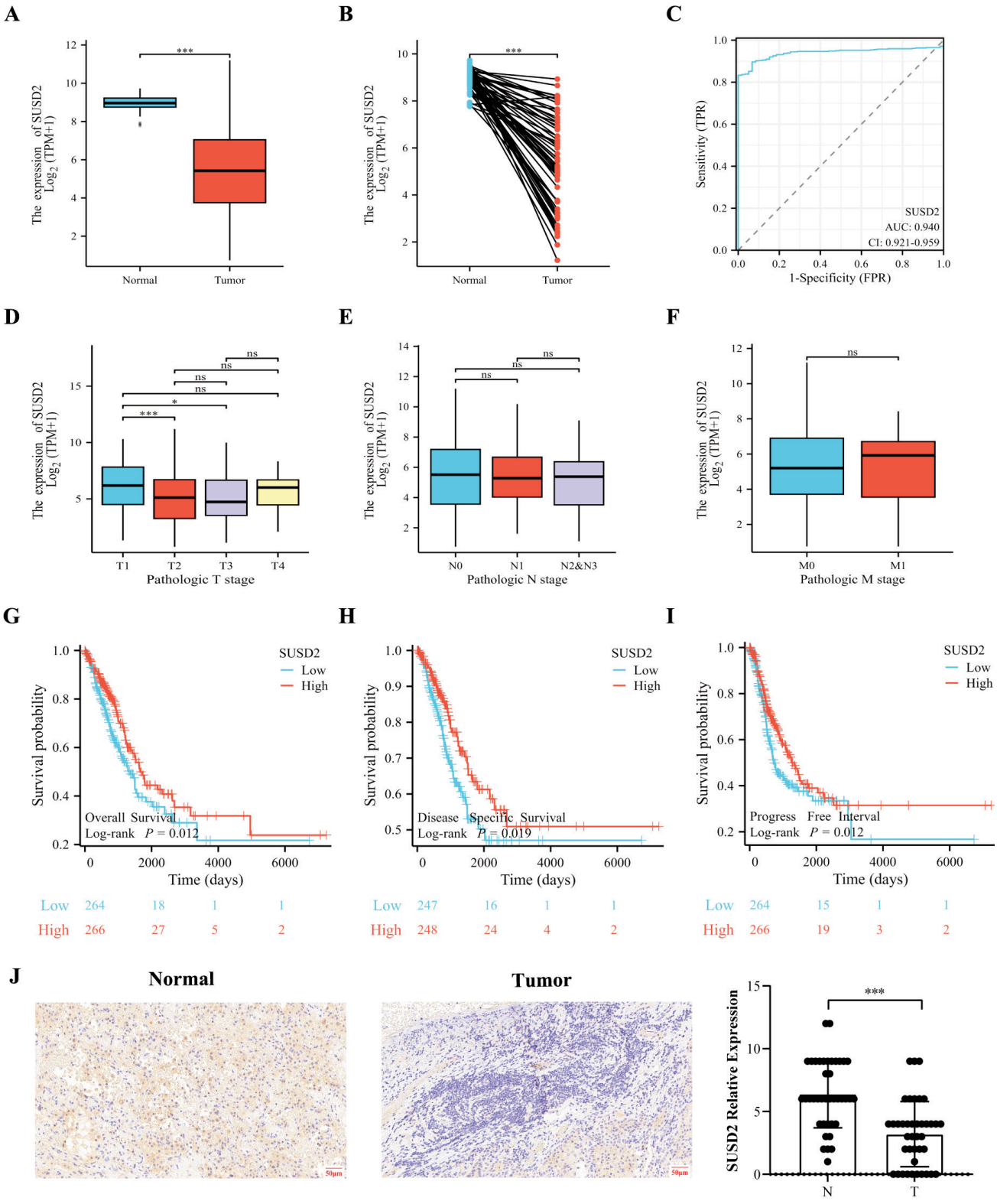

Figure 1. SUSD2 is significantly downregulated in LUAD and serves as a diagnostic and prognostic biomarker. **A,B**) SUSD2 expression is downregulated at both the mRNA and protein levels in LUAD tissues compared to normal lung tissues. **C**) Receiver operating characteristic (ROC) curve analysis demonstrates the high diagnostic accuracy of SUSD2 for distinguishing LUAD from normal tissues. **D-F**) Correlation analysis of SUSD2 expression with clinicopathological features (T, N, M stage); lower SUSD2 expression correlates with higher T stage, but not with N or M stage. **G-I**) Kaplan-Meier survival curves show that patients with low SUSD2 expression have significantly worse overall survival (OS), disease-specific survival (DSS), and progression-free interval (PFI). **J**) Representative immunohistochemistry (IHC) images confirm the reduction of SUSD2 protein expression in LUAD tissues vs adjacent non-tumor tissues. ***p<0.001.

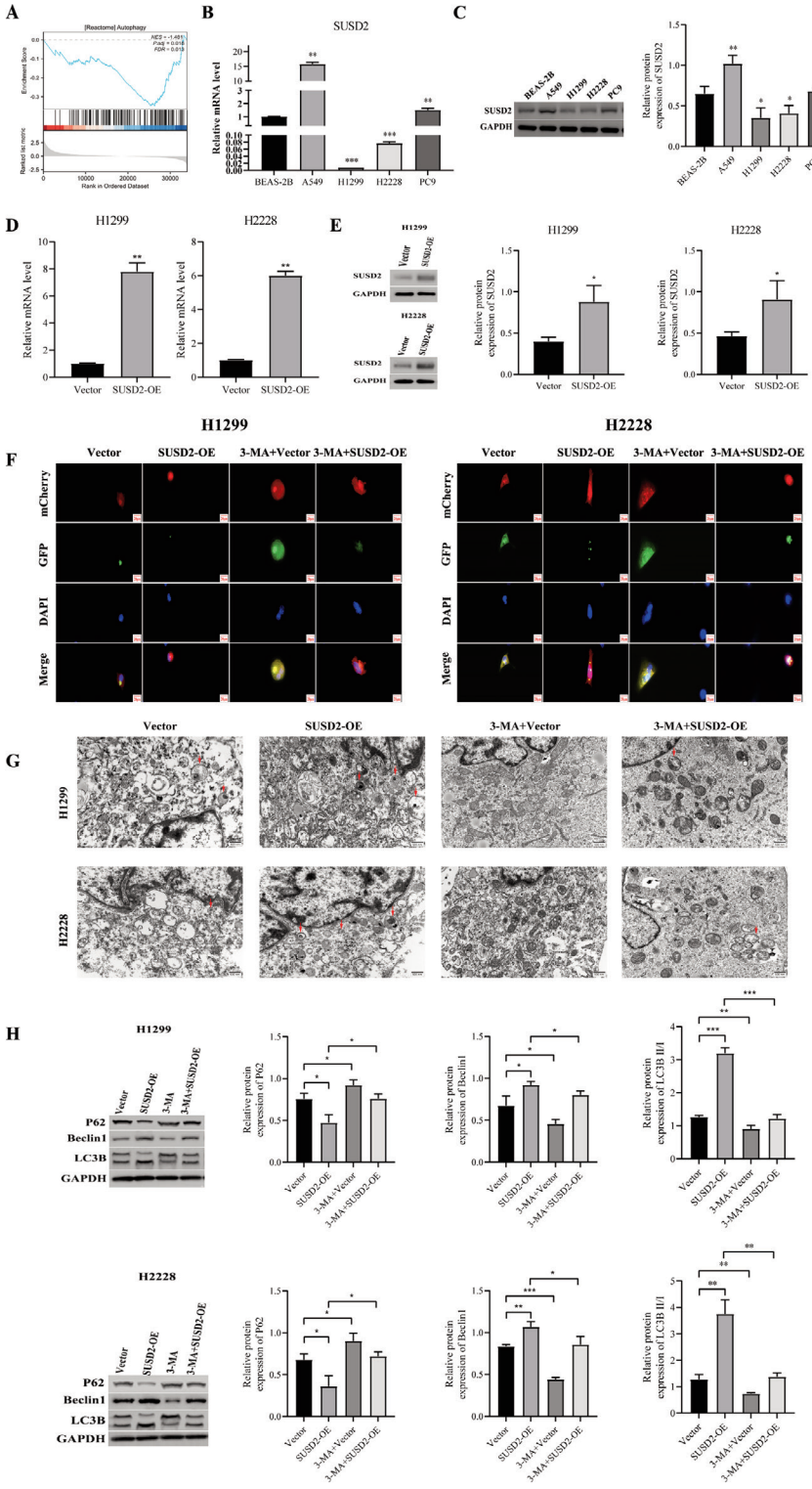

Figure 2. SUSD2 expression varies among LUAD cell lines and is enriched in autophagy-related pathways. **A**) Gene Set Enrichment Analysis (GSEA) plot showing significant enrichment of SUSD2-correlated genes in autophagy-related gene sets. **B,C**) Basal mRNA (**B**) and protein (**C**) expression levels of SUSD2 in a normal bronchial epithelial cell line (BEAS-2B) and a panel of LUAD cell lines, as determined by qRT-PCR and Western blot, respectively. **D,E**) Validation of SUSD2 overexpression efficiency in stably transfected H1299 and H2228 cells by qRT-PCR and Western blot. **F,G**) SUSD2 overexpression promotes autophagic activity; representative immunofluorescence images (**F**) and transmission electron microscopy micrographs (G) show increased autophagic flux in SUSD2-OE cells, which is partially attenuated by co-treatment with the autophagy inhibitor 3-methyladenine (3-MA). **H**) Western blot analysis of key autophagy markers confirms the pro-autophagic role of SUSD2; SUSD2-OE decreases P62 and increases Beclin-1 and LC3B-II levels, changes that are partially reversed upon 3-MA treatment. *p<0.05, **p<0.01, ***p<0.001.

ated in the 3-MA + SUSD2-OE group. (Figure 2H).

These results collectively demonstrate that SUSD2 overexpression enhances autophagy in LUAD cells, an effect that is attenuated by autophagy inhibitors, indicating a regulatory role of SUSD2 in autophagy within LUAD.

SUSD2 overexpression inhibits proliferation and colony formation of lung adenocarcinoma cells *via* autophagy and promotes cell apoptosis

To investigate the impact of SUSD2 overexpression on the proliferative capacity of lung adenocarcinoma cells, CCK-8 assays, colony formation assays, and apoptosis assays were conducted in H1299 and H2228 cell lines after transfection. CCK-8 assay demonstrated that SUSD2 overexpression significantly reduced cell viability compared to control groups in both cell lines, CCK-8 assays were performed on A549 and PC9 cells following knockdown, and the results showed that SUSD2 knockdown significantly increased the viability of both cell lines compared with the control group (*Supplementary Figure 1E*), indicating that SUSD2 effectively inhibits cell proliferation. Conversely, pharmacological inhibition of autophagy with 3-MA treatment substantially increased cell viability. Importantly, co-treatment with SUSD2-OE and 3-MA maintained significantly higher cell viability than SUSD2-OE treatment alone, though still lower than the control group (Figure 3A).

Consistent with these findings, colony formation assays revealed a significant reduction in the number of colonies formed in the SUSD2-OE group compared to the control group. Treatment with 3-MA significantly promoted colony formation, while the SUSD2-OE + 3-MA group exhibited more colonies than the SUSD2-OE group ($p<0.001$; Figure 3B), indicating that autophagy inhibition partially reverses the suppressive effect of SUSD2 overexpression on clonogenic ability.

To assess the influence of SUSD2 on apoptosis, flow cytometric analysis was conducted utilizing Annexin V-FITC/PI double staining. The proportion of apoptotic cells was significantly increased in the SUSD2-OE group compared to the control ($p<0.001$). Conversely, 3-MA treatment led to a marked reduction in apoptosis ($p<0.001$). Notably, the apoptotic rates in the SUSD2-OE + 3-MA co-treatment group remained significantly higher than those in the SUSD2-OE group ($p<0.001$; Figure 3C).

Collectively, these results demonstrate that SUSD2 overexpression inhibits proliferation and colony formation while promoting apoptosis in LUAD cells, and these biological effects can be partially reversed by the autophagy inhibitor 3-MA. This suggests that SUSD2 likely exerts its tumor-suppressive function, at least in part, through activation of the autophagy pathway.

SUSD2 overexpression inhibits lung adenocarcinoma cell migration and invasion *via* autophagy activation

A wound healing assay was employed to evaluate the impact of SUSD2 on the migratory ability of two lung adenocarcinoma cells. The results demonstrated a significant decrease in migration rates at 24 h and 48 h in the SUSD2-OE group compared to the control. In contrast, 3-MA treatment significantly enhanced cell migration, while the SUSD2-OE + 3-MA co-treatment group showed a significant increase in cell migration compared to the SUSD2-OE group in both H1299 and H2228 cell lines (Figure 4A). These data suggest that the inhibitory effect of SUSD2 on cell migration can be partially reversed by autophagy inhibition.

To further examine the role of SUSD2 in tumor invasiveness, transwell invasion assays were conducted in H1299 and H2228 cell lines. The number of invasive cells in the SUSD2-OE groups of the two cell lines was significantly lower than in the controls ($p<0.001$). 3-MA treatment resulted in a significant increase in invasion ($p<0.01$), whereas the SUSD2-OE + 3-MA co-treatment group showed a marked increase in the number of invasive cells compared to the SUSD2-OE single-treatment group. These findings indicate that SUSD2 exerts an inhibitory effect on lung adenocarcinoma cell invasion, potentially through the modulation of autophagy (Figure 4B). In summary, SUSD2 overexpression significantly suppresses the migration and invasion of LUAD cells, and autophagy inhibition partially reverses these phenotypes. This suggests that SUSD2 likely plays an important role in restraining the migratory and invasive capacities of LUAD cells by activating the autophagy pathway.

SUSD2 overexpression suppresses tumor growth *in vivo*

To validate the tumor-suppressive function of SUSD2 *in vivo*, a xenograft tumor model was established in nude mice. Tumor volumes were measured every three days, and after a four-week observation period, tumors were excised for analysis. Compared with the control group, the SUSD2 overexpression group exhibited significantly reduced tumor volume and weight ($p<0.001$; Figure 5A). Employing H&E staining, we found that SUSD2 overexpression provoked profound histopathological alterations, notably reduced tumor cell density, cytoplasmic vacuolization, nuclear fragmentation, and enhanced cellular lysis (Figure 5B). Ki67 and P62 expression levels were markedly downregulated in the SUSD2-OE group (Figure 5 C,D), as confirmed by immunohistochemistry and immunofluorescence, while LC3B and Beclin 1 levels were correspondingly lower in the control group (Figure 5 E,F). Together, these findings evidence the role of SUSD2 in suppressing tumor cell proliferation *in vivo*.

SUSD2 overexpression modulates downstream signaling pathways in lung adenocarcinoma cells

To investigate the molecular mechanism underlying the tumor-suppressive effect of SUSD2, we constructed a PPI network and performed GO and KEGG functional enrichment analyses. Results indicated that SUSD2-associated genes are intricately connected to multiple cancer-related signaling pathways, such as PI3K-AKT, Ras, JAK-STAT, and MAPK pathways (Figure 6 A,B), suggesting that SUSD2 may exert its regulatory functions through these pathways. We then examined the activity of the PI3K/AKT/mTOR pathway in H1299 and H2228 cells. WB analysis, reduced expression of mTOR, p-PI3K, and p-AKT was found in the SUSD2 overexpression group compared with the Vector group, while these levels were elevated in the 3-MA-treated group. Additionally, the levels of mTOR, p-PI3K, and p-AKT were dramatically diminished in the 3-MA + SUSD2-OE group than in the 3-MA group (Figure 6C). These data indicate that SUSD2 overexpression inhibits the activation of the PI3K/AKT/mTOR pathway, and this inhibition can be partially reversed by autophagy suppression. The *in vivo* findings validated that protein expression levels of mTOR, p-PI3K, and p-AKT in xenograft tumors were substantially decreased in the SUSD2 overexpression group as opposed to the control group, as demonstrated by WB analysis. Conversely, these protein levels were elevated in tumors treated with the autophagy inhibitor 3-MA. Moreover, the 3-MA + SUSD2-OE co-treatment group exhibited markedly elevated phosphorylation levels of mTOR, PI3K, and AKT compared to the SUSD2-OE-only group (Figure 6D), indicating that SUSD2 overexpression effectively suppresses the activation of the PI3K/AKT/mTOR signaling pathway *in vivo,* and this regulation is closely linked to autophagy.

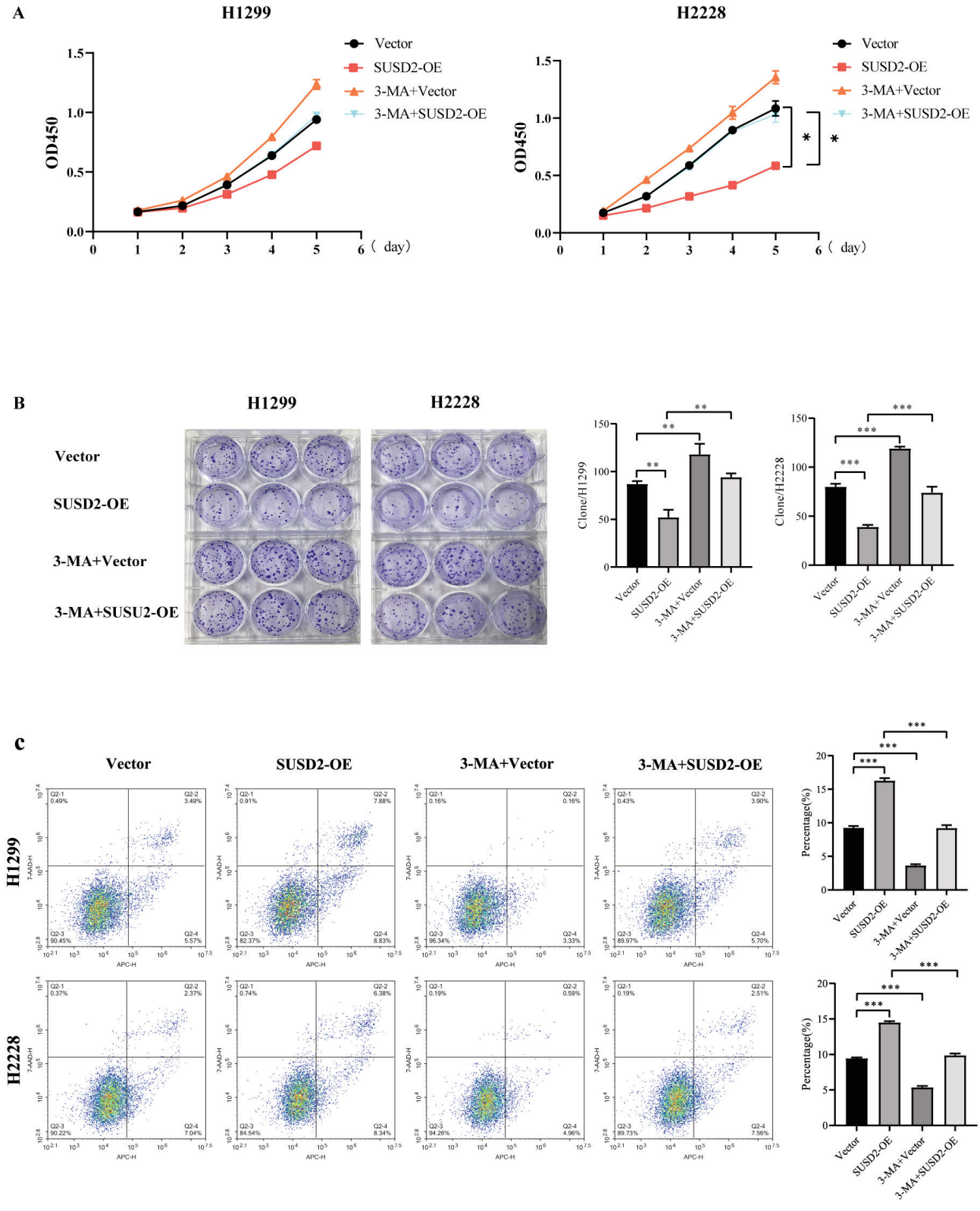

Figure 3. SUSD2 overexpression inhibits proliferation and colony formation of LUAD cells and promotes apoptosis via modulation of autophagy. **A**) Cell viability assessed by CCK-8 assay; SUSD2 overexpression significantly reduces viability, an effect partially rescued by co-treatment with the autophagy inhibitor 3-methyladenine (3-MA). **B**) Colony formation ability evaluated by clonogenic assay; SUSD2-OE cells form fewer colonies, while 3-MA treatment promotes colony growth. **C**) Apoptosis analysis by flow cytometry. SUSD2 overexpression increases the apoptotic rate; although 3-MA co-treatment attenuates this pro-apoptotic effect, the apoptotic rate in the 3-MA + SUSD2-OE group remains higher than in controls. **p*<0.05, ***p*<0.01, ****p*<0.001.

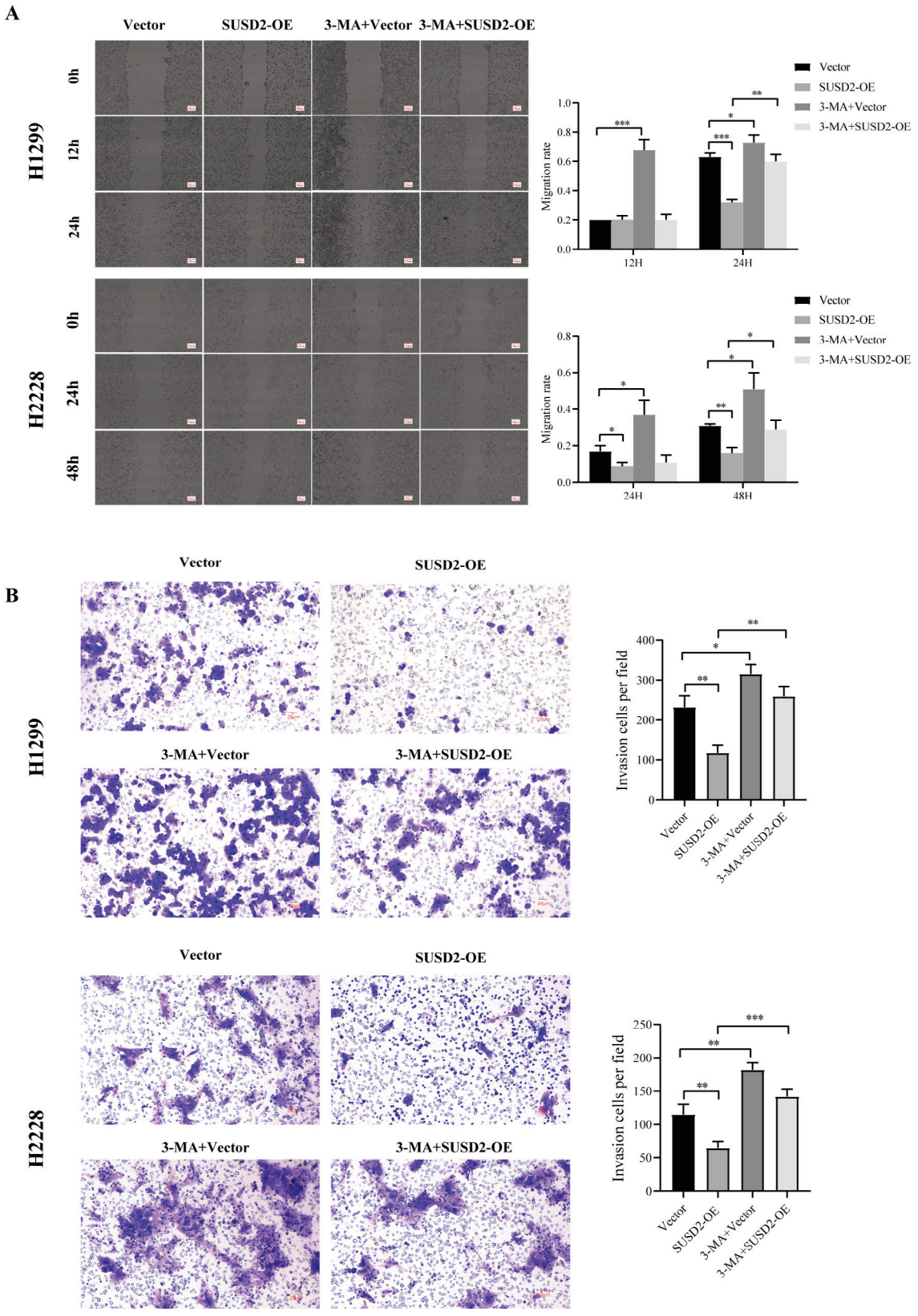

Figure 4. SUSD2 overexpression inhibits LUAD cell migration and invasion by modulating autophagy. **A**) Cell migration ability assessed by wound healing assay. SUSD2 overexpression significantly impedes wound closure, an effect partially reversed upon co-treatment with the autophagy inhibitor 3-methyladenine (3-MA). **B**) Cell invasive capacity evaluated by Transwell Matrigel invasion assay. SUSD2-OE cells exhibit reduced invasiveness, which is also attenuated by 3-MA co-treatment. *p<0.05, **p<0.01, ***p<0.001.

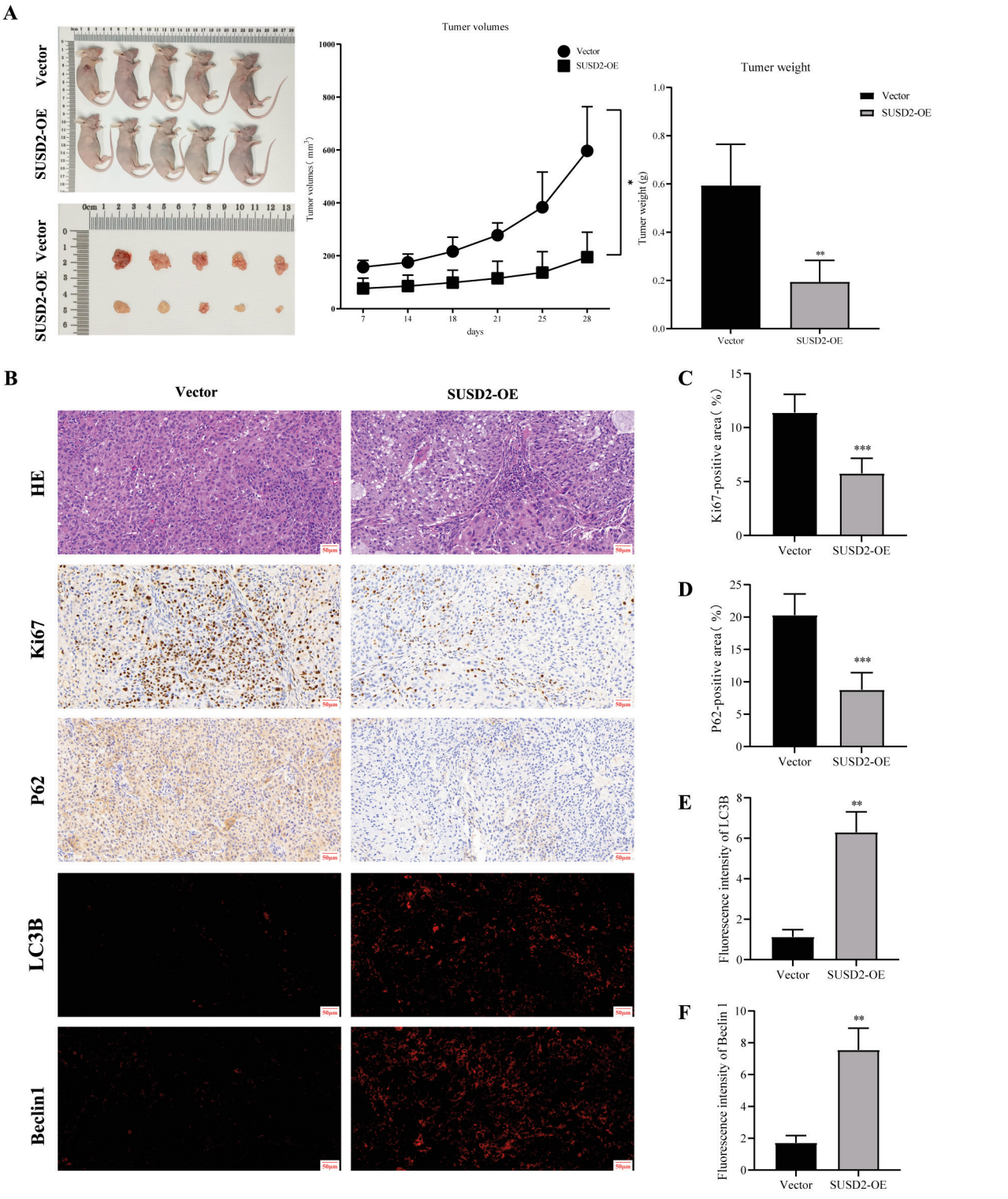

Figure 5. SUSD2 overexpression suppresses tumor growth and proliferation *in vivo.* **A**) Xenograft tumors from the SUSD2-OE group exhibit significantly reduced volume and weight compared to the Vector control group. **B)** Histopathological and molecular analysis of tumor tissues; H&E staining reveals distinct morphological alterations in SUSD2-OE tumors; immunohistochemistry shows decreased expression of Ki67 and P62 in the SUSD2-OE group; immunofluorescence staining demonstrates increased expression of the autophagy markers Beclin 1 and LC3B in SUSD2-OE tumors; 20× magnification. **C**) Quantification of Ki67-positive area (%) from panel B, confirming a significant reduction in the proliferation index within SUSD2-OE tumors. **D**) Quantification of P62-positive area (%) from panel B, indicating enhanced autophagic degradation in SUSD2-OE tumors. **E**) Quantification of LC3B fluorescence intensity from panel B, further supporting heightened autophagic activity in SUSD2-OE tumors. **F**) Quantification of Beclin 1 fluorescence intensity from panel B, demonstrating a significant increase in this key autophagy-initiating protein. *p<0.05, **p<0.01, ***p<0.001.

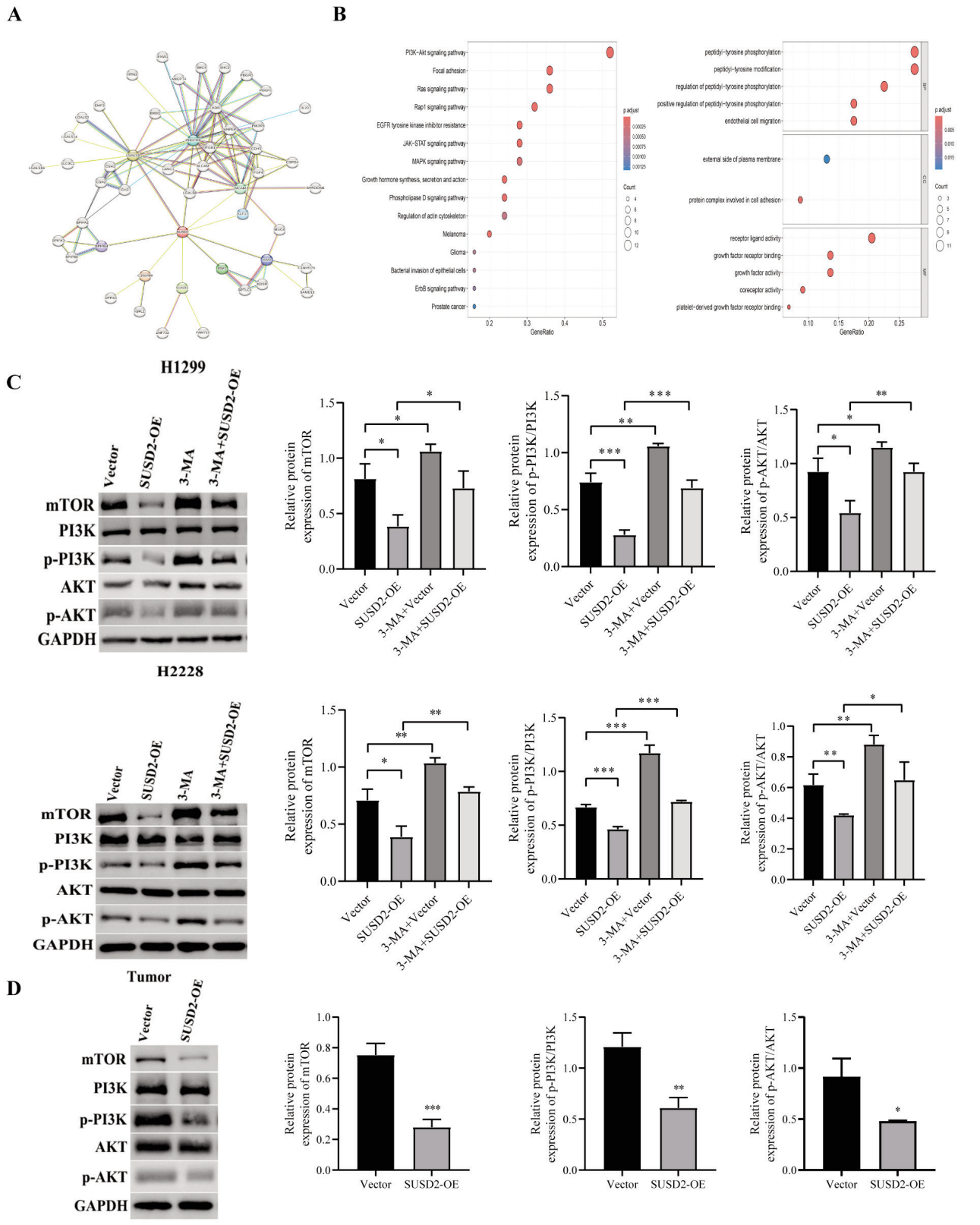

Figure 6. SUSD2 modulates the PI3K-AKT-mTOR signaling pathway in LUAD cells. **A,B**) Gene Ontology and Kyoto Encyclopedia of Genes and Genomes enrichment analyses of SUSD2-co-expressed genes, highlighting significant enrichment in cancer-related pathways including the PI3K-AKT pathway. **C,D**) Western blot analysis validates the pathway modulation; SUSD2 overexpression reduces the protein levels of mTOR and the phosphorylation (activation) of PI3K and AKT; these inhibitory effects are partially reversed upon co-treatment with the autophagy inhibitor 3-methyladenine (3-MA). *p<0.05, **p<0.01, ***p<0.001.

Collectively, these results suggest that SUSD2 overexpression regulates autophagy and suppresses the proliferation, migration, and invasion of lung adenocarcinoma cells by inhibiting the PI3K/AKT/mTOR signaling pathway, indicating that this pathway is a key downstream mechanism through which SUSD2 exerts its tumor-suppressive function.

Discussion

As the predominant subtype of NSCLC, LUAD presents an ongoing therapeutic problem due to its aggressive nature, propensity for metastasis, and poor response to available therapies.[14] Despite notable progress having been made during early diagnosis and targeted therapies, patient prognosis remains poor, particularly in advanced stages. Therefore, it is critical for advancing LUAD management to detect novel biomarkers and uncover their biological functions and underlying regulatory mechanisms.[15,16]

In this study, we identified SUSD2 as a potential tumor suppressor in LUAD. SUSD2 is often overexpressed and correlates with tumor progression, which contrasts with its reported oncogenic roles in other malignancies such as breast, endometrial, and ovarian cancers.[10] Bioinformatics analysis revealed that marked downregulation of SUSD2 in LUAD tissues, in comparison with normal lung tissues. Notably, ROC analysis yielded an AUC of 0.940, indicating its robust diagnostic potential. The prognostic value of SUSD2 in LUAD is confirmed by clinical data evidencing that its low expression corresponds to both advanced T stage and poor overall survival.[17]

The heterogeneous expression of SUSD2 across LUAD cell lines-upregulated in A549 and PC9 but downregulated in H1299 and H2228- reflects the molecular diversity of this malignancy, with different driver mutations potentially influencing basal SUSD2 expression. To address this complexity, we performed complementary loss-of-function studies in high-expressing A549 and PC9 cells. SUSD2 knockdown significantly enhanced proliferation in both cell lines (*Supplementary Figure 1*), consistent with the tumor-suppressive phenotype observed in our gain-of-function studies. These results, together with our overexpression data in H1299 and H2228 cells, provide convergent evidence that SUSD2 functions as a tumor suppressor in LUAD regardless of the underlying mutation profile. The consistent phenotype across different cell line models strengthens our conclusion that SUSD2 downregulation contributes to LUAD progression and suggests that restoring SUSD2 expression may have therapeutic potential across diverse LUAD subtypes.

In vitro studies have demonstrated that SUSD2 overexpression significantly inhibits LUAD cell proliferation, colony formation, migration, and invasion, and promotes apoptosis.[18] These antitumor effects were confirmed *in vivo*, where SUSD2 overexpression suppressed tumor growth and lowered Ki67 expression in xenograft models.[19,20] The tumor-suppressive role for SUSD2 in LUAD contrasts with its reported function as a tumor promoter in certain other cancers, highlighting its context-dependent behavior.[21] This tissue-specific function of SUSD2 may arise from diverse mechanisms, including the tumor microenvironment, interacting partners, and post-translational modifications.[22] Further mechanistic investigation revealed that SUSD2 overexpression promotes autophagy, as evidenced by a consistent increase in autophagosome formation (TEM/IF), promoted LC3-II and Beclin1, and decreased P62, and enhanced autophagic flux. These changes were clearly demonstrated through TEM and IF.[23-25] Intriguingly, the tumor-suppressive phenotype triggered by SUSD2 was incompletely alleviated by the autophagy inhibitor 3-MA, suggesting autophagy activation as a contributor to its antitumor activity.[26] It is suggested that the activation of the autophagy pathway is an important mechanism for SUSD2 to play a tumor suppressor role.

Subsequent investigations evidenced that the PI3K/AKT /mTOR pathway, which is a central regulator of autophagy and tumorigenesis, was regulated by SUSD2.[27] Our results further demonstrate that SUSD2 overexpression reduces the phosphorylation levels of PI3K, AKT, and mTOR (without altering total protein levels) and that autophagy inhibition partially restores the activity of this pathway.[28] These findings demonstrated that SUSD2 alleviates its suppressive effect on autophagy by inhibiting the PI3K/AKT/mTOR signaling cascade, thereby promoting autophagic activity and ultimately suppressing tumor progression, aligning with previous studies.[29]

Remarkably, an essential dichotomy concerning autophagy in LUAD was elucidated here. Whereas autophagy is known to enhance tumor survival when challenged by stress, the results demonstrate a paradoxical effect in LUAD: its reactivation by SUSD2 paradoxically inhibits tumor growth.[30] Not only does this duality exemplify the diverse role of autophagy in cancer biology, but it also emphasizes the requirement for precise, context-dependent modulation strategies.[31]

However, it should be noted that this study has certain limitations. First, while it was demonstrated that SUSD2 is favorable for autophagy induction yet detrimental to tumor progression, have yet to be defined, the precise mechanism of SUSD2 -the specific nodes within the PI3K/AKT/mTOR pathway that SUSD2 directly or indirectly regulate- is still an unresolved issue worthy of in-depth exploration. Future studies employing complementary loss-of-function models are warranted to clarify these mechanistic details.[32-34] Second, the mechanistic connection between SUSD2 and autophagy would be further strengthened by parallel loss-of-function strategies, including genetic knockout or RNA interference (RNAi).[35,36] Third, this research centered on autophagy and the PI3K/AKT/mTOR axis; however, SUSD2 could be implicated in critical pathways of LUAD progression, such as immune modulation, metabolic reprogramming, and EMT.[37,38] Furthermore, the potential epigenetic or transcriptional regulation of SUSD2 merits further exploration. Moreover, future work requires examining whether SUSD2 impacts immune checkpoint expression or the tumor immune microenvironment, potentially uncovering novel therapeutic avenues.[39] Reconstituting SUSD2 expression or mimicking its activity emerges as a promising therapeutic avenue, leveraging its frequent downregulation in LUAD.[40]

In summary, this work uncovers a novel tumor-suppressive function of SUSD2 in LUAD, clarifying a mechanism where it suppresses tumor development through PI3K/AKT/mTOR suppression-induced autophagy.[10,41,42] The clinical relevance of SUSD2 confirms its potential as both a diagnostic and prognostic biomarker as well as a therapeutic target in LUAD.[43] Considering the context-dependent functions of SUSD2, tumor-specific mechanistic studies are critical to guide and advance future precision oncology.[21]

References

1. Luo G, Zhang Y, Rumgay H, Morgan E, Langselius O, Vignat J, et al. Estimated worldwide variation and trends in incidence of lung cancer by histological subtype in 2022 and over time: a population-based study. Lancet Respir Med 2025;13:348-63.

2. Fang W, Li X, Wang Q, Meng X, Zheng W, Sun L, et al. Sacituzumab tirumotecan versus docetaxel for previously treated EGFR-mutated advanced non-small cell lung cancer: multicentre, open label, randomised controlled trial. BMJ 2025;389:e085680.
3. Zhang C, Liu Y, Lu Y, Chen Z, Liu Y, Mao Q, et al. Identification of potential biomarkers for lung adenocarcinoma: a study based on bioinformatics analysis combined with validation experiments. Front Oncol 2024;14:1425895.
4. Gómez-Virgilio L, Silva-Lucero MD, Flores-Morelos DS, Gallardo-Nieto J, Lopez-Toledo G, Abarca-Fernandez AM, et al. Autophagy: a key regulator of homeostasis and disease: an overview of molecular mechanisms and modulators. Cells 2022;11.
5. Liu S, Yao S, Yang H, Liu S, Wang Y. Autophagy: Regulator of cell death. Cell Death Dis 2023;14:648.
6. Wang S, Long H, Hou L, Feng B, Ma Z, Wu Y, et al. The mitophagy pathway and its implications in human diseases. Signal Transduct Target Ther 2023;8:304.
7. Wang Q, Sun Y, Li TY, Auwerx J. Mitophagy in the pathogenesis and management of disease. Cell Res 2026;36:11-37.
8. Hennes D, Rosamilia A, Werkmeister JA, Gargett CE, Mukherjee S. Endometrial SUSD2(+) mesenchymal stem/stromal cells in tissue engineering: advances in novel cellular constructs for pelvic organ prolapse. J Pers Med 2021;11:840.
9. Huang T, Ge S, Huang W, Ma T, Sheng Y, Chen J, et al. AIBP promotes cell proliferation and migration through the ERK1/2-MAPK signaling pathway in hepatocellular carcinoma. Transl Cancer Res 2024;13:4028-41.
10. Bai H, Xian N, Zhao F, Zhou Y, Qin S. The dual role of SUSD2 in cancer development. Eur J Pharmacol 2024;977:176754.
11. Wang F, Li Q, Xie C, Zhu N, Deng Y, Li Y, et al. Dysregulation of SUSD2-CLDN18.2-mediated cell adhesion contributes to lung adenocarcinoma progression associated with chronic low-dose nanoplastics exposure. Ecotoxicol Environ Saf 2025;303:118946.
12. Kuo WT, Lee YC, Yang YF, Cheng CF, Tseng CJ, Tsai KW. Sushi Domain Containing 2 dysfunction contributes to cancer progression in patients with bladder cancer. J Cancer 2024;15:5318-28.
13. Liu J, Tao M, Zhao W, Song Q, Yang X, Li M, et al. Calcium channel α2δ1 is essential for pancreatic tumor-initiating cells through sequential phosphorylation of PKM2. Cell Mol Gastroenterol Hepatol 2023;15: 373-392.
14. Tian Y, Xu L, Li X, Li H, Zhao M. SMARCA4: Current status and future perspectives in non-small-cell lung cancer. Cancer Lett 2023;554:216022.
15. Chen P, Quan Z, Song X, Gao Z, Yuan K. MDFI is a novel biomarker for poor prognosis in LUAD. Front Oncol 2022;12:1005962.
16. Zhang H, Zhang P, Lin X, Tan L, Wang Y, Jia X, et al. Integrative single-cell analysis of LUAD: elucidating immune cell dynamics and prognostic modeling based on exhausted CD8+ T cells. Front Immunol 2024;15:1366096.
17. Chen JW, Dhahbi J. Lung adenocarcinoma and lung squamous cell carcinoma cancer classification, biomarker identification, and gene expression analysis using overlapping feature selection methods. Sci Rep 2021;11:13323.
18. Liu S, Wen C. miR-141-3p promotes retinoblastoma progression via inhibiting sushi domain-containing protein 2. Bioengineered 2022;13:7410-24.
19. Yang C, Zhang J, Ding M, Xu K, Li L, Mao L, et al. Ki67 targeted strategies for cancer therapy. Clin Transl Oncol 2018;20:570-5.
20. Zhang A, Wang X, Fan C, Mao X. The role of Ki67 in evaluating neoadjuvant endocrine therapy of hormone receptor-positive breast cancer. Front Endocrinol (Lausanne) 2021;12:687244.
21. Zhou D, Zhang J, Deng X, Lu X, Liu X, Yu J, et al. SUSD2 hypersialylation promotes early lung adenocarcinoma progression by driving ECM remodeling and pro-tumorigenic fibroblast activation. Cancer Lett 2025;633:217995.
22. Moreno-Sanchez PM, Scafidi A, Salvato I. SUSD2-IL-2 receptor interaction hinders antitumoral CD8(+) T-cell activity: Implications for cancer immunotherapy. Allergy 2023;78:3035-7.
23. Liu WJ, Ye L, Huang WF, Guo LJ, Xu ZG, Wu HL, et al. p62 links the autophagy pathway and the ubiquitin-proteasome system upon ubiquitinated protein degradation. Cell Mol Biol Lett 2016;21:29.
24. Prerna K, Dubey VK. Beclin1-mediated interplay between autophagy and apoptosis: New understanding. Int J Biol Macromol 2022;204:258-73.
25. Bartkowiak K, Mohammadi PM, Nissen P, Werner S, Agorku D, Andreas A, et al. Discovery of a sushi domain-containing protein 2-positive phenotype in circulating tumor cells of metastatic breast cancer patients. Sci Rep 2025;15:3913.
26. Sun X, Meng H, Xiao J, Liu F, Du J, Zeng H. Pretreatment of 3-MA prevents doxorubicin-induced cardiotoxicity through inhibition of autophagy initiation. Toxicology 2023;490: 153512.
27. Peng Y, Wang Y, Zhou C, Mei W, Zeng C. PI3K/Akt/mTOR pathway and its role in cancer therapeutics: are we making headway? Front Oncol 2022;12:819128.
28. Mondal K, Posa MK, Shenoy RP, Roychoudhury S. KRAS mutation subtypes and their association with other driver mutations in oncogenic pathways. Cells 2024;13.
29. Alves CL, Ditzel HJ. Drugging the PI3K/AKT/mTOR pathway in ER+ breast cancer. Int J Mol Sci 2023;24.
30. Zhang J, Li MY, Lu X, Liu QX, Zhou D, Yang GX, et al. CWHM-1008 induces apoptosis and protective autophagy through the Akt/mTOR axis in LUAD cells. J Oncol 2021;2021:5548128.
31. Li X, He S, Ma B. Autophagy and autophagy-related proteins in cancer. Mol Cancer 2020;19:12.
32. Sun K, Luo J, Guo J, Yao X, Jing X, Guo F. The PI3K/AKT/mTOR signaling pathway in osteoarthritis: a narrative review. Osteoarthritis Cartilage 2020;28:400-9.
33. Leiphrakpam PD, Are C. PI3K/Akt/mTOR signaling pathway as a target for colorectal cancer treatment. Int J Mol Sci 2024;25.
34. Yoshida J, Ohishi T, Momose I, Ohba SI, Kurosawa K, Harakawa A, et al. SUSD2 promotes metastasis and primary tumor growth in pancreatic cancer cells via integrin-FAK signaling activation. Cancer Sci 2026;117:711-26.
35. Gorsek Sparovec T, Markert UR, Reif P, Schoell W, Moser G, Feichtinger J, et al. The fate of human SUSD2+ endometrial mesenchymal stem cells during decidualization. Stem Cell Res 2022;60:102671.
36. Zhao B, Gong W, Ma A, Chen J, Velegraki M, Dong H, et al. SUSD2 suppresses CD8(+) T cell antitumor immunity by targeting IL-2 receptor signaling. Nat Immunol 2022;23:1588-99.
37. Wei X, Li X, Hu S, Cheng J, Cai R. Regulation of ferroptosis in lung adenocarcinoma. Int J Mol Sci 2023;24.
38. Jiang M, Zhou X, Feng Y, Ding P, Li J, Lu D, et al. DNMT3a promotes LUAD cell proliferation and metastasis by activating the HDAC7 signalling pathway. Int J Biol Sci 2025;21:1585-602.

39. Khanmohammadi M, Mukherjee S, Darzi S, Paul K, Werkmeister JA, Cousins FL, et al. Identification and characterisation of maternal perivascular SUSD2(+) placental mesenchymal stem/stromal cells. Cell Tissue Res 2021;385:803-15.
40. Wu Y, Duan Y, Li X, Zhao R, Lan B, Zhang X, et al. CBX8 together with SET facilitates ovarian carcinoma growth and metastasis by suppressing the transcription of SUSD2. Mol Cancer Res 2022;20:1611-22.
41. Zhang L, Xiong Y, Zhang J, Feng Y, Xu A. Systematic proteome-wide Mendelian randomization using the human plasma proteome to identify therapeutic targets for lung adenocarcinoma. J Transl Med 2024;22:330.
42. Hao C, Wei Y, Meng W, Zhang J, Yang X. PI3K/AKT/mTOR inhibitors for hormone receptor-positive advanced breast cancer. Cancer Treat Rev 2025;132:102861.
43. Zhang L, Cui Y, Zhou G, Zhang Z, Zhang P. Leveraging mitochondrial-programmed cell death dynamics to enhance prognostic accuracy and immunotherapy efficacy in lung adenocarcinoma. J Immunother Cancer 2024;12:e010008.

Online Supplementary Material
Supplementary Figure 1. Knockdown of SUSD2 enhances cell viability in lung adenocarcinoma (LUAD) cells.
Supplementary Table 1. Clinical patients' information

Received: 6 February 2026. Accepted: 20 April 2026.

Licensee PAGEPress, Italy
European Journal of Histochemistry 2026; 70:4544
doi:10.4081/ejh.2026.4544